Inorg. Chem. **2008**, *47*, 6162−6172

Ligand-Bound $S = {}^1/_2$ FeMo-Cofactor of Nitrogenase: Hyperfine Interaction Analysis and Implication for the Central Ligand X Identity

Vladimir Pelmenschikov,* David A. Case, and Louis Noodleman

The Scripps Research Institute, Department of Molecular Biology TPC-15, 10550 North Torrey Pines Road, La Jolla, California 92037

Received November 19, 2007

Broken symmetry density functional theory (BS-DFT) has been used to address the hyperfine parameters of the single atom ligand **X**, proposed to be coordinated by six iron ions in the center of the paramagnetic FeMo-cofactor (FeMoco) of nitrogenase. Using the **X** = N alternative, we recently found that any hyperfine signal from **X** would be small (calculated $A_{iso}(\mathbf{X} = {}^{14}N) = 0.3$ MHz) due to both structural and electronic symmetry properties of the [Mo−7Fe−9S−**X**] FeMoco core in its resting $S = {}^3/_2$ state. Here, we extend our BS-DFT approach to the $2e^-$ reduced $S = {}^1/_2$ FeMoco state. Alternative substrates coordinated to this FeMoco state effectively perturb the electronic and/or structural symmetry properties of the cofactor. Using an example of an allyl alcohol ($H_2C{=}CH{-}CH_2{-}OH$) product ligand, we consider three different binding modes at single iron site and three different BS-DFT spin state structures and show that this binding would enhance the key hyperfine signal $A_{iso}(\mathbf{X})$ by at least 1 order of magnitude ($3.8 \leq A_{iso}(\mathbf{X} = {}^{14}N) \leq 14.7$ MHz), and this result should not depend strongly on the exact identity of **X** (nitrogen, carbon, or oxygen). The interstitial atom, when the nucleus has a nonzero magnetic moment, should therefore be observable by ESR methods for some ligand-bound FeMoco states. In addition, our results illustrate structural details and likely spin-coupling patterns for models for early intermediates in the catalytic cycle.

1. Introduction

To benefit from the ∼78% abundance of molecular nitrogen in the atmosphere, nature has developed a class of prokaryotes called diazotrophs. Hosted in vivo solely by diazotrophs, the nitrogenase metalloenzyme performs a multielectron/multiproton reduction of relatively inert dinitrogen (N_2) into ammonia (NH_3). An iron−molybdenum cofactor[1] FeMoco, which is unique to nitrogenases, Figure 1, is the site for reduction of N_2 and a variety of nonphysiological substrates.

In 2002, electron density was resolved inside the FeMoco iron trigonal prismane ([6Fe]) which can be ambiguously associated with a single nitrogen, carbon, or oxygen atom.[2] Despite intensive efforts from both the experimental and theoretical sides, the identity of this interstitial atom (denoted **X**) is still open to debate.[3] **X** = N has been supported by most theoretical studies,[4,5] but experiments using electron−nuclear double resonance (ENDOR) or electron spin−echo envelope modulation (ESEEM) have not detected any observable signals from $^{14,15}N$ in the resting $S = {}^3/_2$ state of FeMoco (called M^N or E_0, proposed [$Mo^{4+}4Fe^{2+}3Fe^{3+}$] oxidation state for the metals).[6−8] Isotropic hyperfine signals

* To whom correspondence should be addressed. E-mail: vovan@scripps.edu. Present address: Scientific Computing & Modelling NV, Theoretical Chemistry, Vrije Universiteit, De Boelelaan 1083, NL-1081 HV Amsterdam, The Netherlands.

(1) (a) Shah, V. K.; Brill, W. J. *Proc. Natl. Acad. Sci. U.S.A.* **1977**, *74*, 3249–3253. (b) Rawlings, J.; Shah, V. K.; Chisnell, J. R.; Brill, W. J.; Zimmermann, R.; Munck, E.; Orme-Johnson, W. H. *J. Biol. Chem.* **1978**, *253*, 1001–4.

(2) Einsle, O.; Tezcan, F. A.; Andrade, S. L.; Schmid, B.; Yoshida, M.; Howard, J. B.; Rees, D. C. *Science* **2002**, *297*, 1696–700.

(3) Howard, J. B.; Rees, D. C. *Proc. Natl. Acad. Sci. U.S.A.* **2006**, *103*, 17088–17093.

(4) (a) Hinnemann, B.; Norskov, J. K. *Topics in Catalysis* **2006**, *37*, 55–70. (b) Dance, I. *Inorg. Chem.* **2006**, *45*, 5084–5091. (c) Cao, Z. X.; Jin, X.; Zhang, Q. N. *J. Theoret. Comput. Chem.* **2005**, *4*, 593–602. (d) Huniar, U.; Ahlrichs, R.; Coucouvanis, D. *J. Am. Chem. Soc.* **2004**, *126*, 2588–2601. (e) Hinnemann, B.; Norskov, J. K. *J. Am. Chem. Soc.* **2004**, *126*, 3920–3927. (f) Vrajmasu, V.; Munck, E.; Bominaar, E. L. *Inorg. Chem.* **2003**, *42*, 5974–5988. (g) Hinnemann, B.; Norskov, J. K. *J. Am. Chem. Soc.* **2003**, *125*, 1466–1467. (h) Dance, I. *Chem. Commun.* **2003**, 324–325.

(5) Lovell, T.; Liu, T.; Case, D. A.; Noodleman, L. *J. Am. Chem. Soc.* **2003**, *125*, 8377–83.

(6) Lee, H. I.; Sorlie, M.; Christiansen, J.; Yang, T. C.; Shao, J. L.; Dean, D. R.; Hales, B. J.; Hoffman, B. M. *J. Am. Chem. Soc.* **2005**, *127*, 15880–15890.

10.1021/ic7022743 CCC: $40.75
Published on Web 06/26/2008

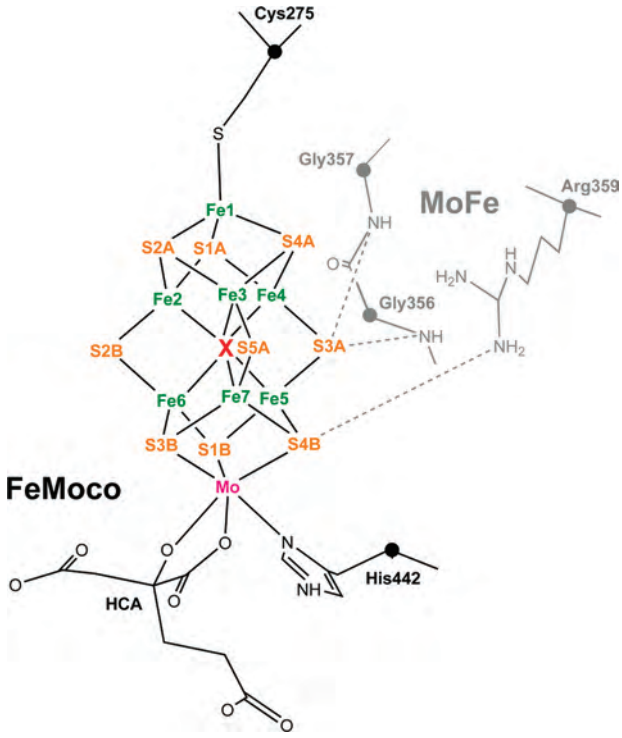

Figure 1. FeMoco of nitrogenase with its interstitial ligand **X** coordinated by the six iron atoms Fe2−7. The covalent ligands (in black) to the cofactor [Mo−7Fe−9S−**X**] core are Cys275, His442, and homocitrate (HCA). First-shell MoFe protein ligands (in gray) Arg359 and Gly356/357 are tentative origins of N1 and N2 nitrogen hyperfine signals, respectively (section 1 of the text). FeMoco atom namings follow their crystallographic notation.[2] C_α carbons are given as spheres.

of $A_{iso}(^{14}N) = 1.05$ MHz and $A_{iso}(^{14}N) = 0.5$ MHz were reported for the MoFe protein containing FeMoco bound, but these signals were not seen for the cofactor extracted into N-methyl formamide (NMF) solvent.[6,7,9] Called N1 and N2, the two above modulations were assigned to nitrogens of the polypeptide, tentatively side chain nitrogen of Arg359 and backbone nitrogen of Gly356/357 (Figure 1). No strong natural abundance in ^{13}C signals have been detected either,[6] precluding **X** = C identification. Recent ENDOR/ESEEM measurements put upper bounds on the interstitial atom hyperfine signal, if present: for **X** = N, $A_{iso}(\mathbf{X} = {}^{14}N) \leq 0.05$ MHz, and for **X** = C, $A_{iso}(\mathbf{X} = {}^{13}C) \leq 0.1$ MHz.[8] These upper bounds essentially reflect the state of the art sensitivity of the most-recent experiments. No ^{17}O ENDOR/ESEEM assessment for an **X** = O candidate has yet been reported; the ^{17}O experimental setup would be prohibitively expensive.

Using density functional theory (DFT) calculations in combination with the broken symmetry (BS) approach for spin coupling, small $A_{iso}(\mathbf{X} = {}^{14}N/{}^{13}C/{}^{17}O) = 0.3/1.0/0.1$ MHz were obtained recently for **X** candidates nitrogen, carbon, and oxygen in the resting FeMoco oxidation state.[8] The absence of a strong **X** hyperfine signal was rationalized as an outcome of the electronic and structural symmetry properties of the [6Fe] prismane, formed by the six irons adjacent to **X**: a cancelation of [6Fe] irons electron spin densities in a 3↑:3↓ (3 − 3 = 0) spin coupling, in concert with the symmetry of the prismane structure results in a very small point spin density $\rho = 0.4 \times 10^{-2}$ au (atomic units, or electrons per cubic bohr) at the **X** nucleus location. In contrast, 4↑:2↓ (4 − 2 = 2) spin coupling of the 6 prismane irons yields significantly larger $\rho = -2.5 \times 10^{-2}$ au. Notably, all of the 10 simple (parallel or antiparallel) spin alignments (called broken symmetry (BS) states, section 2.3) available for the resting-state FeMoco possess either a 3↑:3↓ or a 4↑:2↓ pattern within [6Fe][10] (Chart 2, the first BS*x* column). For the two lowest-energy BS states, BS7 (≃0.0 kcal/mol, 3↑:3↓) and BS6 (+6.6 kcal/mol, 4↑:2↓), our calculated $A_{iso}(\mathbf{X} = {}^{14}N)$ values are 0.3 and 9.6 MHz, respectively, [8] (Figure 2). For the resting state FeMoco, BS7 spin coupling is therefore now favored because it (i) gives the lowest energy among the BS states and (ii) conforms to the lack of an observed **X** hyperfine signal. Whereas our $A_{iso}(\mathbf{X} = {}^{14}N) = 0.3$ MHz for BS7 is several times larger than the experimental $A_{iso}(\mathbf{X} = {}^{14}N) = 0.05$ MHz upper bound,[8] combined uncertainties in the BS-DFT approach may easily result in a ∼0.3 MHz absolute error in the computed **X** isotropic hyperfine constant.

Chart 1. Proposed Fe6-η^2(C=C) Ferracycle Binding Mode of Allyl Alcohol (CH_2=CH−CH_2−OH) at Fe6 of FeMoco

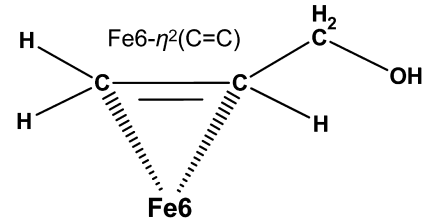

We thus expect that the hyperfine coupling of **X** to the FeMoco spin can be significantly enhanced by either electronic or structural symmetry perturbations of the [6Fe] prismane. A ligand binding at one of the [6Fe] irons would potentially lead to such perturbations. However, no species are known to coordinate at the iron prismane of the cofactor in its resting state. Some substrates can be trapped in a paramagnetic $S = 1/2$ state, generated via $2e^-$ reduction and, presumably, $2H^+$ protonation of the cofactor.[11,12] Notably, the $2e^-$ reduced FeMoco itself has been characterized as $S = 1/2$ state[12] in the absence of any extra substrate. Also, ^{57}Fe ENDOR hyperfine data for $S = 1/2$ states named "S_{EPR1}" and "lo-CO", which trap different ligands C_2H_4 (resulting from reductive binding of C_2H_2) and CO, correspondingly, indicate that the electronic properties, including magnetic coupling on ^{57}Fe, of these two intermediates are similar.[6] On the basis of the above considerations, we will first assume that the electronic structure of the [Mo−7Fe−9S−**X**] core is gener-

(7) Lee, H. I.; Benton, P. M. C.; Laryukhin, M.; Igarashi, R. Y.; Dean, D. R.; Seefeldt, L. C.; Hoffman, B. M. *J. Am. Chem. Soc.* **2003**, *125*, 5604–5605.
(8) Lukoyanov, D.; Pelmenschikov, V.; Maeser, N.; Laryukhin, M.; Yang, T. C.; Noodleman, L.; Dean, D. R.; Case, D. A.; Seefeldt, L. C.; Hoffman, B. M. *Inorg. Chem.* **2007**, *46*, 11437–11449.
(9) Thomann, H.; Morgan, T. V.; Jin, H.; Burgmayer, S. J. N.; Bare, R. E.; Stiefel, E. I. *J. Am. Chem. Soc.* **1987**, *109*, 7913–7914.
(10) Lovell, T.; Li, J.; Liu, T. Q.; Case, D. A.; Noodleman, L. *J. Am. Chem. Soc.* **2001**, *123*, 12392–12410.
(11) Barney, B. M.; Lee, H. I.; Dos Santos, P. C.; Hoffmann, B. M.; Dean, D. R.; Seefeldt, L. C. *Dalton Trans.* **2006**, 2277–2284.
(12) Dos Santos, P. C.; Igarashi, R. Y.; Lee, H. I.; Hoffmann, B. M.; Seefeldt, L. C.; Dean, D. R. *Acc. Chem. Res.* **2005**, *38*, 208–214.

Chart 2. Spin Coupling Alignments (BS States) Available for the Seven Iron Sites of FeMoco in the Resting State (BSx, $x = 1-10$), and $2e^-$ Reduced State (BSx, $x = 1-10$; BS$x-$, $x = 1-10$; BSNx, $x = 1-6$)[a]

x	BSx (4↑:3↓)	BSx- (3↑:4↓)	BSNx (5↑:2↓)
1	23.7		
2	0.0	16.9	
3	9.2	11.7	
4	11.3		
5	10.6	16.9	
6	3.3	5.6	
7	0.2		
8	5.0	9.8	
9	7.7	13.7	
10	5.8	7.7	

[a] The energies (kcal/mol), when available, are given for the $2e^-$ reduced state relatively to the most-stable spin coupling, BS2.

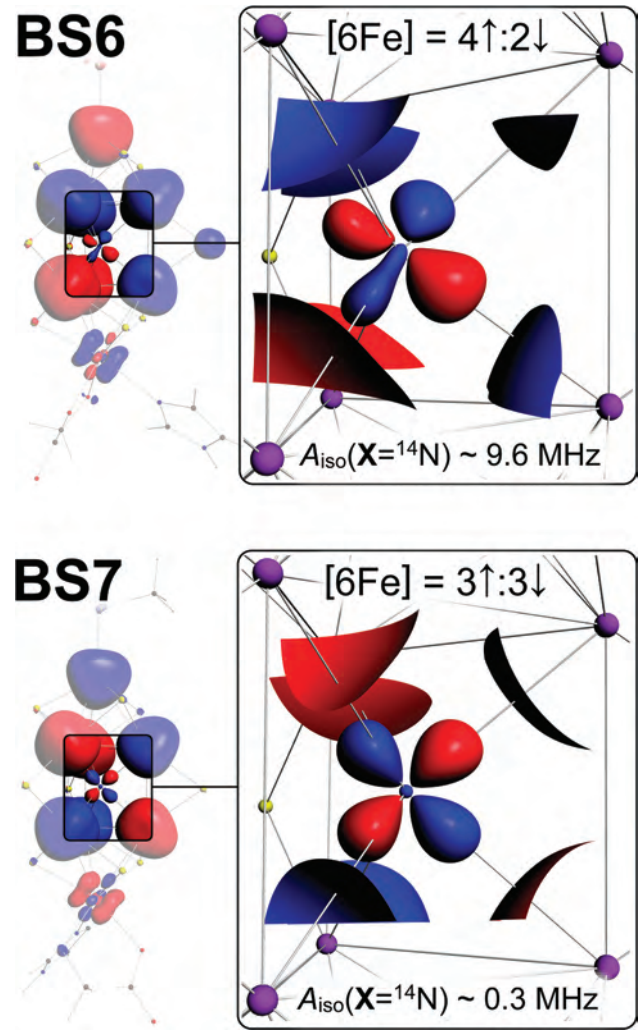

Figure 2. 3D spin density maps for the resting state FeMoco BS6 and BS7 spin couplings. Point spin density $\rho = \pm 0.01$ au (atomic units, or electron per cubic bohr) isosurfaces correspond to the hyperfine coupling $A_{iso}(\mathbf{X} = {}^{14}\mathrm{N}) \sim 5$ MHz. Blue/red surfaces are for the positive/negative ρ contour values, correspondingly. For BS7, the node ($\rho < 0.01$ au) of the spin density at the **X** position is manifested in small $A_{iso}(\mathbf{X} = {}^{14}\mathrm{N}) \sim 0.3$ MHz. Contrary to BS7, $\rho > 0.01$ au at the **X** position for BS6, manifested in $A_{iso}(\mathbf{X} = {}^{14}\mathrm{N}) \sim 9.6$ MHz. 3D isosurfaces were generated using *ADF View* based on our recent DFT calculations.[8]

ally similar for all relevant $S = {}^1/_2$ $2e^-$ reduced FeMoco core species, regardless of ligand binding. We will provide our further support for this assumption below.

Elucidating ligand binding modes at FeMoco is anticipated to shed light onto the nitrogenase reaction mechanism. Despite intensive research in this area, there is limited information at the molecular level about precise geometry of species when bound to FeMoco. Substrates featuring unsaturated C=C/C≡C bonds are thought to coordinate at the [6Fe] prismane face, formed by iron numbers 2, 3, 6, and 7 (all of the atom names here follow their crystallographic notations).[13] In this study, we consider allyl alcohol (CH_2=CH−CH_2−OH), proposed to coordinate to FeMoco as a Fe6-η^2(C=C) ferracycle product upon reductive binding

(13) Igarashi, R. Y.; Dos Santos, P. C.; Niehaus, W. G.; Dance, I. G.; Dean, D. R.; Seefeldt, L. C. *J. Biol. Chem.* **2004**, *279*, 34770–5.

of propargyl alcohol ($CH{\equiv}C{-}CH_2{-}OH$),[12–16] (Chart 1). Notably, in the context of the Thorneley−Lowe kinetic scheme[17] using E_nH_k notation for the nitrogenase catalytic intermediates, the allyl alcohol-bound cofactor would be described as the E_4H_4 state; here, n is the number of electrons and k is the number of protons delivered to the MoFe protein. The electron inventory concept[6] relates the number of electrons accepted by the MoFe protein from the iron protein (n) to the net number of electrons that are delivered to FeMoco (m), plus those transmitted to the substrate (s), and also counting the electrons transferred to FeMoco from the P cluster (p): $n + p = m + s$. With the assumption that $p = 0$, we obtain $n = 4$ for the allyl alcohol-bound FeMoco using $m = 2$ ($2e^-$ reduced FeMoco) and $s = 2$ ($2e^-$required to reduce the propargyl alcohol substrate). Similarly, $k = 4$ results from the two protons delivered to FeMoco and two protons required to complete the reduction of the propargyl alcohol.

Prior to introducing the ligand-bound complex, FeMoco spin couplings compatible with $S = 1/2$ and $2e^-$ reduced oxidation level are considered in detail. We optimize three alternative conformations of allyl alcohol intermediate and predict the corresponding A_{iso}(**X**) values. Finally, the correlation between our calculated and ^{57}Fe ENDOR experimental hyperfine parameters for the seven FeMoco iron sites is provided.

2. Computational Details

2.1. Modeling. Coordinates for the FeMoco structure were taken from the 1.16 Å resolution 1M1N PDB file.[2] The structural model includes [Mo-7Fe-9S-**X**] core and its covalent ligands Cys275, His442, and *R*-homocitrate (HCA) (Figure 1) simplified to methylthiolate, imidazole, and glycolate ($^-OCH_2{-}COO^-$), respectively. Whereas the **X** = N^{3-} (also referred to as N_X below) alternative was used for the interstitial atom, our results should qualitatively hold for **X** = C^{4-}/O^{2-} as well. The charge model corresponds to formal oxidation states [$Mo^{4+}3Fe^{3+}4Fe^{2+}$] for the metals in the resting state of FeMoco, as proposed elsewhere.[5,18] The $2e^-$ reduced cofactor considered here would therefore correspond to [$Mo^{4+}1Fe^{3+}6Fe^{2+}$] formal oxidation states, assuming that the molybdenum remains Mo^{4+} (also section 3.1). The sulfurs S2B and S3A (Figure 1) were selected as protonation sites, in agreement with some recent studies favoring μ_2S−H FeMoco protonations[19,20] and our own earlier work.[21] The ligand-bound FeMoco was constructed first placing allyl alcohol ($CH_2{=}CH{-}CH_2{-}OH$) at Fe6 (as Fe6-η^2(C=C) ferracycle, Chart 1) and then geometry-optimizing the complex. The starting geometry of the cofactor was intentionally perturbed to allow three different local minima, as discussed in section 3.4 below.

2.2. Density Functional Methods. The calculations were done using the parametrization of electron gas data given by Vosko, Wilk, and Nusair (VWN, formula version V)[22] for the local density approximation (LDA), and the corrections proposed in 1991 by Perdew and Wang (PW91)[23] for the generalized gradient approximation (GGA), as implemented in the Amsterdam Density Functional (ADF)[24] package. During the geometry optimizations by ADF, triple-ζ plus polarization (TZP) basis sets were used for iron and molybdenum metal sites, whereas double-ζ plus polarization (DZP) basis sets were used for other atoms. The inner shells of iron ($1s^22s^22p^6$) and molybdenum($1s^22s^22p^63s^23p^64s^23d^{10}$) were treated by the frozen-core approximation. Accurate single point wave functions, used to report the properties of the ligand-bound FeMoco state (relative energies, spin densities and spin populations, and hyperfine couplings), were obtained using TZP basis set on all of the atoms, with the frozen core used only for molybdenum as described above. Effects of the polar protein environment were considered using conductor-like screening model (COSMO)[25] with the dielectric constant set to $\varepsilon = 4.0$.

2.3. Spin Coupling and Broken-Symmetry (BS) States. The FeMoco of nitrogenase includes eight metal sites, all of them potentially carrying unpaired electrons. For this type of system a set of the site spin vectors, satisfying a given set of metal oxidation states and a given total spin, is generally not unique. For the resting state FeMoco ([$Mo^{4+}3Fe^{3+}4Fe^{2+}$], $S = 3/2$), 10 spin alignments were constructed earlier[5,10] (Chart 2, BS*x* column) using a simple spin-collinear (up ↑ or down ↓) approach for three high spin ferric (Fe^{3+}, d^5, $S = 5/2$) and 4 high-spin ferrous (Fe^{2+}, d^6, $S = 2$) sites. This approach yields all of the spin alignments which bear $\Sigma M_{S_i} = M_S = S_t = 3/2$ total FeMoco spin projection, implying that iron-site spin vectors $\boldsymbol{S}_i$ are collinear with the total spin vector $\boldsymbol{S}_t$, $M_{S_i} = S_i$, $i = 1...7$; notably, the [Mo−7Fe−9S−**X**] core possesses pseudo C_3 structural symmetry around the rotational axis formed by the atoms Fe1, **X**, and molybdenum. Three rotamers for some of the spin alignments can be found. The presence of the covalent terminal ligands (Cys275, His442, HCA) to [Mo−7Fe−9S−**X**] results in small variations of these rotamer energies by ∼1 kcal/mol.[10] When the protein environment is included as well (via Poisson−Boltzmann electrostatics approach), the rotamer energies are found to be split by ∼2 kcal/mol at most using our earlier modeling.[26] We therefore consider only single rotamer for each spin alignment here. Because these spin orderings do not represent pure $S = 3/2$ spin states but rather broken-symmetry (BS) states;[27] the nomenclature BS1 to BS10 was originally applied. We have now developed a utility code that generates BS states automatically. This utility takes user-defined number of spin sites and their types as input. For every site type, a set of its possible formal ionic charges Q_i is given, and for every ionic charge a set of possible formal site spin projections M_{S_i} is defined. A programmed combinatorial search is then performed, with the two restraints set for the total charge ($\sum Q_i = Q_t$) and total spin projection ($\sum M_{S_i} = M_S = S_t$). We used this utility to address spin couplings for FeMoco at its $2e^-$ reduced oxidation level (section 3.1 below). Notably, the application of our new utility

(14) Lee, H. I.; Igarashi, R. Y.; Laryukhin, M.; Doan, P. E.; Dos Santos, P. C.; Dean, D. R.; Seefeldt, L. C.; Hoffman, B. M. *J. Am. Chem. Soc.* **2004**, *126*, 9563–9569.
(15) Dance, I. *J. Am. Chem. Soc.* **2004**, *126*, 11852–11863.
(16) Dos Santos, P. C.; Mayer, S. M.; Barney, B. M.; Seefeldt, L. C.; Dean, D. R. *J Inorg Biochem* 2007.
(17) Thorneley, R. N. F.; Lowe, D. J. *J. Biol. Inorg. Chem.* **1996**, *1*, 576–580.
(18) Yoo, S. J.; Angove, H. C.; Papaefthymiou, V.; Burgess, B. K.; Munck, E. *J. Am. Chem. Soc.* **2000**, *122*, 4926–4936.
(19) Kastner, J.; Blochl, P. E. *J. Am. Chem. Soc.* **2007**, *129*, 2998–3006.
(20) Dance, I. *Biochemistry* **2006**, *45*, 6328–6340.
(21) Lovell, T.; Li, J.; Case, D. A.; Noodleman, L. *J. Am. Chem. Soc.* **2002**, *124*, 4546–4547.
(22) Vosko, S. H.; Wilk, L.; Nusair, M. *Can. J. Phys.* **1980**, *58*, 1200–1211.
(23) Perdew, J. P.; Chevary, J. A.; Vosko, S. H.; Jackson, K. A.; Pederson, M. R.; Singh, D. J.; Fiolhais, C. *Phys. Rev. B* **1992**, *46*, 6671–6687.
(24) Velde, G. T.; Bickelhaupt, F. M.; Baerends, E. J.; Guerra, C. F.; Van Gisbergen, S. J. A.; Snijders, J. G.; Ziegler, T. *J. Comput. Chem.* **2001**, *22*, 931–967.
(25) Pye, C. C.; Ziegler, T. *Theor. Chem. Acc.* **1999**, *101*, 396–408. (a) Klamt, A.; Jonas, V. *J. Chem. Phys.* **1996**, *105*, 9972–9981. (b) Klamt, A. *J. Phys. Chem.* **1995**, *99*, 2224–2235. (c) Klamt, A.; Schuurmann, G. *J. Chem. Soc., Perkin Trans. 2* **1993**, 799–805.
(26) Lovell, T.; Li, J.; Case, D. A.; Noodleman, L. *J. Biol. Inorg. Chem.* **2002**, *7*, 735–749.
(27) Noodleman, L. *J. Chem. Phys.* **1981**, *74*, 5737–5743.

Table 1. Assigned Oxidation States, Formal Spin Vector Magnitudes S_i, Their Projection Values M_{S_i}, and Calculated Spin Projection Coefficients K_i for the Seven Iron Sites in $2e^-$ Reduced FeMoco

i	oxidation state	$M_{S_i} = \pm S_i$	K_i
1	2+	+2	+12/11
2	2+	−2	−180/143
3	2.5+	−9/4	−405/286
4	2.5+	−9/4	−405/286
5	2+	+2	+22/15
6	2+	+1[a]	+16/15
7	2+	+2	+22/15
Sum		+1/2	+1

[a] Exception: $M_{S_i} \neq S_i = 2$ for site $i = 6$ due to canting (section 3.2).

confirmed that the set of formerly introduced spin couplings BS1 to BS10[10] is complete for the resting state FeMoco; for the $2e^-$ reduced FeMoco, new BS states were found (Chart 2). When using ADF, a desired BS state was achieved first converging the ferromagnetic high-spin (7↑:0↓, HS) state ($S = {}^{31}/_2$ for the resting, and $S = {}^{29}/_2$ for the $2e^-$ reduced-state FeMoco), then exchanging α (↑) and β (↓) electron densities associated with the desired spin-down iron atoms and finally restarting the calculation. For both collinear and noncollinear spin states, the connection between the BS-state spin-density distribution and the hyperfine properties is provided by the spin coupling scheme and spin projection coefficients (eqs 1−6 below). Unless specifically stated (section 3.1), all of the BS states were geometry optimized using the methodology described above in section 2.2.

2.4. Calculation of the Hyperfine Coupling Parameters. Electronic spin densities obtained from ADF[28] were used to calculate hyperfine coupling $\boldsymbol{A}$ tensors. The isotropic contribution $A_{\mathrm{iso}}^{\mathrm{UBS}}$ to the calculated unrestricted broken symmetry (UBS) (raw) $\boldsymbol{A}$ tensor, also called the Fermi or contact interaction, is proportional to the point electron spin density, $|\Psi(0)|^2$ at the nucleus,

$$A_{\mathrm{iso}}^{\mathrm{UBS}} = (8\pi/3h) g_e \beta_e g_N \beta_N |\Psi(0)|^2 / 2S_t \tag{1}$$

where S_t is the total electron spin of the system. In case of an **X** atom confined within [6Fe] prismane of FeMo-co, this raw result must be projected onto the total system spin. Quantitatively, this can be expressed as follows:[29,30]

$$A_{\mathrm{iso}}(\mathrm{X}) = \frac{1}{6} \sum_{i=2,3...7} (|K_i/S_i|S_t) A_{\mathrm{iso}}^{\mathrm{UBS}}(\mathbf{X}) = P_{\mathrm{X}} A_{\mathrm{iso}}^{\mathrm{UBS}}(\mathbf{X}) \tag{2}$$

where $A_{\mathrm{iso}}(\mathbf{X})$ is the calculated spin-coupled isotropic hyperfine parameter (which can be compared to experiment) and the sum runs over the six Fe ions adjacent to **X**. Here, K_i is a spin projection coefficient of the local Fe site spin $\boldsymbol{S}_i$ onto the total FeMoco spin $\boldsymbol{S}_t$:

$$\mathrm{K}_i = \langle \boldsymbol{S}_i \boldsymbol{S}_t \rangle / \langle \boldsymbol{S}_t \boldsymbol{S}_t \rangle \tag{3}$$

The K_i to be used in eq 3 were obtained applying spin projection chain and sum rules,[10,29] (eqs 4 and 5 below). The chain rule allows expressing K_i as the product of a site-spin projection coefficient onto a subunit spin, K_i^q, and the subunit spin projection coefficient onto the total system spin, K_q^t:

$$K_i = K_i^t = K_i^q K_q^t \tag{4}$$

The sum rule states that the sum of the projection coefficients over all the sites is one:

$$\sum_{i=1,2,3...7} \mathrm{K}_i = 1 \tag{5}$$

Transition-metal hyperfine parameters directly computed by DFT are generally known to be prone to errors.[31] For this reason, semiempirical calculations for the ^{57}Fe site hyperfine couplings (A_i^{calcd}, Tables 1 and 2) were performed based on the following equation,[30]

$$\mathrm{A}_i^{\mathrm{calcd}} = K_i (|P_{3\mathrm{d}}(\mathrm{Fe}_i)|/2S_i) a_i^{\mathrm{ionic}} = K_i d_{\mathrm{B}}(\mathrm{Fe}_i) a_i^{\mathrm{ionic}} \tag{6}$$

where $P_{3\mathrm{d}}(\mathrm{Fe}_i)$ is the calculated 3d Mulliken spin population of site i, and $d_{\mathrm{B}}(\mathrm{Fe}_i) = |P_{3\mathrm{d}}(\mathrm{Fe}_i)|/2S_i$ is the covalency factor, which is the ratio of the $P_{3\mathrm{d}}(\mathrm{Fe}_i)$ spin population to the $2S_i$ maximum expected spin population in the valence-bond limit. $d_{\mathrm{B}}(\mathrm{Fe}_i) = 1$ in the ionic limit and decreases with increasing covalency, $d_{\mathrm{B}}(\mathrm{Fe}_i) < 1$. For a given BS state, $d_{\mathrm{B}}(\mathrm{Fe}_i) \geq 1$ indicates an S_i assignment inconsistent with the electronic structure; $d_{\mathrm{B}}(\mathrm{Fe}_i)$ values for some relevant structures of the present study are discussed in the text and listed in Table S3 in the Supporting Information. a^{ionic} in eq 6 is the intrinsic site hyperfine parameter for a purely ionic iron, which depends on the iron oxidation state:[30]

$$\begin{aligned} a^{\mathrm{ionic}}(\mathrm{Fe3^+}) &= -31.0 \text{ MHz} \\ a^{\mathrm{ionic}}(\mathrm{Fe2.5^+}) &= -32.5 \text{ MHz} \\ a^{\mathrm{ionic}}(\mathrm{Fe2^+}) &= -34.0 \text{ MHz} \end{aligned} \tag{6a}$$

This procedure was originally developed to interpret iron hyperfine constants in iron−sulfur ([FeS]) clusters[30,32] and is expected to provide a good qualitative picture of how couplings from the individual sites are manifested in the experimental (coupled) spectrum. The quality of the semiempirical iron hyperfine parameters can be assessed by considering the sum of the calculated A_i^{calcd} over all the sites, called a_{test}:

$$a_{\mathrm{test}} = \sum_{i=1,2,3...7} A_i^{\mathrm{calcd}} \tag{7}$$

For a number of [FeS] clusters, a_{test} values in the range of −16 to −25 MHz were previously found.[30] Values significantly outside of this range may be indicative of incorrect spin coupling.

3. Results and Discussion

The organization of this section is as follows. We first consider the electronic structure of the ligand-free $2e^-$ reduced FeMoco using BS-DFT approach (with no μ_2S cluster sites protonated at this stage). Spin alignments compatible with the $S = {}^1/_2$ and $2e^-$ reduced oxidation level are constructed and assessed by their relative energies. Using the selected BS state, a spin coupling model in $2e^-$ reduced FeMoco is developed. On the basis of the ligand-free electronic structure, we then construct and optimize three alternative local minima of the allyl alcohol intermediate. The interstitial atom hyperfine coupling parameter, $A_{\mathrm{iso}}(\mathbf{X})$, is calculated for $\mathbf{X} = {}^{14}$N in all of the intermediate alternatives. We then provide further justification of our results comparing the calculated semiempirical iron hyperfine parameters to the relevant ^{57}Fe ENDOR data. Finally, we

(28) van Lenthe, E.; van der Avoird, A.; Wormer, P. E. S. *J. Chem. Phys.* **1998**, *108*, 4783–4796.
(29) Noodleman, L.; Peng, C. Y.; Case, D. A.; Mouesca, J. M. *Coord. Chem. Rev.* **1995**, *144*, 199–244.
(30) Mouesca, J. M.; Noodleman, L.; Case, D. A.; Lamotte, B. *Inorg. Chem.* **1995**, *34*, 4347–4359.
(31) Kaupp, M.; Bühl, M.; Malkin, V. G. *Calculation of NMR and EPR Parameters: Theory and Applications*; Wiley-VCH: Weinheim, Germany, 2004.
(32) Mouesca, J. M.; Noodleman, L.; Case, D. A. *Inorg. Chem.* **1994**, *33*, 4819–4830.

Table 2. Calculated Structural (Fe_i-N_X Internuclear Distances), Electronic ($P(Fe_i)$ Net Electron Spin Populations), and Semiempirical Hyperfine (A_i^{calcd}) Parameters of the Seven Iron Sites of FeMoco for Allyl Alcohol Intermediate Structures **1**, **2**, and **3** (Figure 4) [a]

	Fe_i-N_X (Å)[b]			$P(Fe_i)$ (*e*)			A_i^{calcd}(MHz)			A_i^{exp}	
i	**1**	**2**	**3**	**1**	**2**	**3**	**1**	**2**	**3**	value (MHz)	site type
1				2.9	2.7	2.8	−27.1	−25.4	−26.2	−23to−26	β_4
2	2.0	2.0	2.1	−2.6	−3.1	−2.9	27.7	33.1	31.1	32	α_3
3	2.0	2.0	2.0	−2.6	−3.0	−2.7	26.4	30.4	27.2	32	α_3
4	2.0	1.9	1.9	−2.7	−2.7	−2.4	27.7	27.9	24.6	32	α_3
5	2.0	1.8	1.9	2.6	2.2	2.1	−32.3	−27.5	−25.8	−33	α_4
6	2.3	3.4	2.0	1.1	3.0	2.0	−9.9	−26.9	−18.2	−18	β_3
7	2.0	1.9	2.0	2.6	2.7	2.6	−32.2	−33.2	−32.7	−33	α_4
Sum				1.3	1.8	1.6	−19.7	−21.6	−20.0	−11to−14	

[a] The reported Fe_i-N_X distances precision is set to 0.1 Å to simplify their comparison (higher precision structural data is available from the Supporting Information). [b] The electronic state is BS2 and the spin coupling is canted at Fe6 ($S_6 = 2$, $M_{S_6} = 1$; Figure 3). The matching experimental hyperfine coupling constants[6] and their spectroscopic notations[18] for the ethylene bound state S_{EPR1} are given in the last two columns.

test three alternative BS states for each of the three local minima of the ligand-bound FeMoco.

3.1. Iron Spin Alignment in 2e⁻ reduced FeMoco. Combined analysis of ^{95,97}Mo ENDOR and Mo EXAFS data suggests that the molybdenum is spinless in $2e^-$ reduced FeMoco.[33] Our results on the ligand-bound FeMoco species **1**−**3** considered below in section 3.3 show that the calculated molybdenum spin densities correspond to approximately half of the unpaired electron based on the Mulliken spin populations (Table S4 in the Supporting Information). This can be interpreted as a mixed oxidation state molybdenum between Mo^{4+} (d^2, $S = 0$) and Mo^{3+} (d^3, $S = 1/2$). If Mo^{4+} oxidation favored by the experiment is assumed, only the seven iron sites would participate in spin coupling for both resting ($[Mo^{4+}3Fe^{3+}4Fe^{2+}]$, $S = 3/2$) and $2e^-$ reduced ($[Mo^{4+}1Fe^{3+}6Fe^{2+}]$, $S = 1/2$) FeMoco states. Because the three iron (Fe_5, Fe_6, and Fe_7) spin vectors neighboring to molybdenum are large, the effect of transferring $1e^-$ to Mo^{4+} from Fe^{2+} and then antiferromagnetically coupling Mo^{3+} ($S = 1/2$) to Fe^{3+} ($S = 5/2$ or $3/2$) will not change the overall spin-coupling picture significantly.

For the resting state, there are only 10 simple collinear spin alignments satisfying formal $[Mo^{4+}3Fe^{3+}4Fe^{2+}]$ oxidation states for the metals and $M_S = 3/2$ when constraining the iron sites to high-spin (ferric Fe^{3+}, d^5, $S = 5/2$ and ferrous Fe^{2+}, d^6, $S = 2$); section 2.3 and Chart 2. Notably, all 10 BS*x* states, $x = 1...10$, have a 4↑:3↓ spin coupling pattern. In $2e^-$ reduced [FeS] clusters, ferric Fe^{3+} site is often considered as a part of $2Fe^{2.5+}$ mixed-valence pair.[33] The $2e^-$ reduced-state FeMoco valences can then be reformulated as $[Mo^{4+}2Fe^{2.5+}5Fe^{2+}]$. For a $Fe^{2.5+}$ site, the formal high spin is given as $S = 1/2(2 + 5/2) = 9/4$, which is the average between $S = 2$ of Fe^{2+} and $S = 5/2$ of Fe^{3+}. Our automated procedure (section 2.3) predicts that, for $[Mo^{4+}2Fe^{2.5+}5Fe^{2+}]$, no BS states with total $M_S = 1/2$ can be found when accepting only collinear high-spin mixed-valence ($2Fe^{2.5+}$, $S = 9/2$) and ferrous (Fe^{2+}, $S = 2$) sites. The combinatorial search satisfying $\sum M_{Si} = M_S = S_t = 1/2$ is successful only if *at least one* Fe^{2+} site spin vector projection becomes $M_{S_i} = 1$. This can be achieved if the corresponding ferrous site is (i) high-spin canted, so that $\boldsymbol{S}_i$ and $\boldsymbol{S}_t$ vectors are no longer collinear or (ii) converted into the true intermediate spin $S_i = 1$.Three subsets of BS states were found for the $2e^-$ reduced FeMoco, Chart 2: (i) the 10 classic BS states, accessible if *one* $M_{S_i} = 1$ Fe^{2+} site is present; (ii) 10 inverted 3↑:4↓ BS states (named BS1− to BS10−, "−" for inverted), allowed if *two* $M_{S_i} = 1$ Fe^{2+} sites are present; (iii) finally, 6 new 5↑:2↓ BS states (named BSN1 to BSN6, "N" for new), requiring five $M_{S_i} = 1$ Fe^{2+} sites. Notably, decomposing the mixed-valence $2Fe^{2.5+}$ into Fe^{3+} & Fe^{2+} pair and considering whole $[Mo^{4+}1Fe^{3+}6Fe^{2+}]$ valences instead produces the same set of BS states.

The relative energies within each BS subset (BS*x*, BS*x*−, or BSN*x*) are largely influenced by the number of antiferromagnetic interactions between the μ_2S and μ_3S sulfur-bridged iron pairs, as noted before for the resting FeMoco state.[10] The number of the formal intermediate spin projection $M_{S_i} = 1$ ferrous sites is, however, different in the three BS subsets, and grows in line BS (1) → BS− (2) → BSN (5), which introduces another factor in relative energies. BS− states were found to be typically higher in energy than classic BS states (these two subsets however overlap on the energy scale, Chart 2). We were unable to converge any of the six BSN states, probably due to the significant instability of this subset. All attempts to achieve a DFT solution for a 5↑:2↓ coupling (after exchanging α (↑) and β (↓) electron densities as described in section 2.3) resulted in either BS (4↑:3↓) or BS− (3↑:4↓) states. The convergence of BS*x*− states is not trivial as well: no solutions for BS*x*− numbers $x = 1$, 4, and 7 were found. The final result is that for $S = 1/2$ $2e^-$ reduced FeMoco, BS2 coupling gives the lowest energy (≡0.0 kcal/mol) with BS7 only 0.2 kcal/mol less stable (Chart 2). The accuracy of the modern DFT methods does not allow us to discriminate between BS2 and BS7 on the basis of such a small energies difference only; in sections 3.4 and 3.5 below, we provide additional arguments favoring BS2 versus BS7.

Our comparative results on BS, BS−, and BSN relative energies are in good agreement with a recent DFT study,[19] which used a two-component spinor description of the wave function (nonbiased to conventional collinear spin calculations). In this study, it was found that noncollinear spin arrangements in FeMoco result in energetically unfavorable states. Alternatively, BS- and BSN subsets provide a larger number of true intermediate ($S = 1$) or low ($S = 0$) spin ferrous sites than BS, whereas the high-spin ($S = 2$) Fe^{2+} is

(33) Lee, H. I.; Hales, B. J.; Hoffman, B. M. *J. Am. Chem. Soc.* **1997**, *119*, 11395–11400.

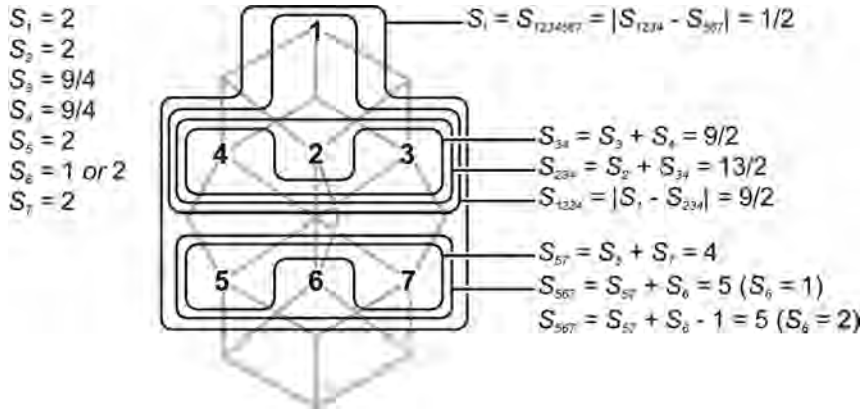

Figure 3. The presently used nested spin vector coupling model for the seven iron sites in $2e^-$ reduced FeMoco. Iron site numbering is given. The two options for the Fe6 site spin $S_6 = 2$ (main assignment, canting at Fe6) and $S_6 = 1$ (alternative assignment, intermediate spin at Fe6) are considered.

generally favored in the tetrahedral coordination environment of iron−sulfur ([FeS]) clusters.[34]

3.2. Spin Coupling and Projection Coefficients. Iron spin-projection coefficients K_i (section 2.4) must be obtained to calculate hyperfine parameters. Spin-projection coefficients have been calculated earlier for $[Mo^{4+}1Fe^{3+}6Fe^{2+}]$, $S = {}^3/_2$, BS6[10] and recently for $[Mo^{4+}3Fe^{3+}4Fe^{2+}]$, $S = {}^3/_2$, BS7.[8] Analogous approach is applied below for the $2e^-$ reduced FeMoco core $[Mo^{4+}1Fe^{3+}6Fe^{2+}]$, $S = {}^1/_2$, BS2. To use this approach, tentative S_i values for the seven iron centers must be assigned first.

There is high degree of spin delocalization in FeMoco, as confirmed by generally homogeneous $P(Fe_i)$ iron Mulliken spin populations, $i = 1...7$. There is also non-negligible spin transfer from irons to other atoms (Table S4 in the Supporting Information). This is confirmed by deviations of the $P(Fe_i)$ sum from 1 (corresponding to one net unpaired electron for $S = {}^1/_2$), (Table 2) and deviations of the covalency factors $d_B(Fe_i)$ from 1 (Table S3 in the Supporting Information). Spin delocalization and transfer preclude us from assigning site charges and spins based only on $P(Fe_i)$ values. The two following guidelines were used to do the assignment for the iron sites: (i) to comply with BS2 coupling, $M_{S_i} = 1$ is necessary for at least one of the ferrous sites (above in section 3.1); here, we choose to place the $M_{S_i} = 1$ spin vector at Fe6, which is the unique ligand-binding site and might be the subject to spin canting ($S_6 = 2$, $M_{S_6} = 1$) or intermediate spin ($S_6 = 1$, $M_{S_6} = 1$) (ii) if *only one* $M_{S_i} = 1$ ferrous site is allowed, $2Fe^{2.5+}$ mixed-valence pair spin vectors must be antiparallel to the total spin vector, as follows from the combinatorial search; for BS2 this implies that the two $Fe^{2.5+}$ sites are among the three spin-down (↓) Fe numbers 2, 3, and 4; Fe3 and Fe4 were presently selected. The four remaining sites ($i = 1, 2, 5, 7$) are then high-spin ferrous. We used a coupling model where spin vectors are generally collinear (not canted), so that adding spins S_A and S_B would yield either $S_{AB} = S_A + S_B$ or $|S_A - S_B|$. The main coupling model however involves canting at the single Fe6 site ($S_6 = 2$, $M_{S_6} = 1$), see the list of iron spins S_i in Table 1; an alternative S_i assignment does not involve canting at Fe6 but requires its conversion into the intermediate spin ($S_6 = 1$, $M_{S_6} = 1$) ferrous site (Table S1 in the Supporting Information). The graphic representation showing the nested structure of the current spin coupling model is given in Figure 3. To derive the spin-projection coefficients K_i, spin projection chain (eq 4) and sum (eq 5) rules were applied to our coupling model. The resultant K_i values for the main spin assignment ($S_6 = 2$ case) are given in Table 1 and for the alternative assignment ($S_6 = 1$ case) in Table S1 in the Supporting Information. According to eq 2, the scaling factor for the central **X** atom isotropic hyperfine $A_{iso}(\mathbf{X})$ is then $P_{\mathbf{X}} = 0.32$ for the main spin assignment and $P_{\mathbf{X}} = 0.36$ for the alternative.

3.3. Allyl Alcohol binding Modes at FeMoco and $A_{iso}(\mathbf{X})$. Alkyne species were proposed to bind reductively at Fe-2,3,4,7 face of the [6Fe] prismane, most probably at Fe6, resulting in Fe6-η^2(C═C) ferracycle[13–16] (section 1 and Chart 1). Even when limited to Fe6-η^2(C═C) coordination, multiple configurations are available for allyl alcohol-bound FeMoco, depending on the relative orientation of the ligand and the cofactor, as well as FeMoco conformation itself.[15] Using the methodology described above in section 2.2, we have analyzed three local minima (named **1**, **2**, and **3**) for allyl alcohol Fe6-η^2(C═C) coordination at FeMoco (Figure 4). The C═C bond of the allyl alcohol was initially placed on the extension of the Fe6−**X** bond, perpendicular to it. The ligand was rotated around Fe6−**X** axis in a manner to receive the most stabilization from allyl−OH···S2B hydrogen bonding. This type of alkene coordination at FeMoco approximately persisted through the geometry optimizations and has been considered as favorable by a recent combined DFT and molecular mechanics (MM) study.[13] We will first assume that [Mo−7Fe−9S−**X**] core electronic structures of a ligand-bound and (hypothetic) nonbound $2e^-$ reduced cofactor states are similar (section 1), so that they will share the same lowest-energy spin coupling of the iron sites. BS2 spin alignment, shown to be the most favorable in section 3.1 above, was therefore used for the intermediate. A limited test of this assumption is provided in section 3.5 below.

Notably, spin populations of the Fe6-bound alkene carbon atoms were found to be small, $|P(C_i)| < 0.1e$ ($i = 1, 2$; Figure 4) for the intermediate alternatives **1**−**3** considered below, and this observation favors Fe6−C π-(C═C) versus σ(C)

(34) Beinert, H.; Holm, R. H.; Munck, E. *Science* **1997**, *277*, 653–659.

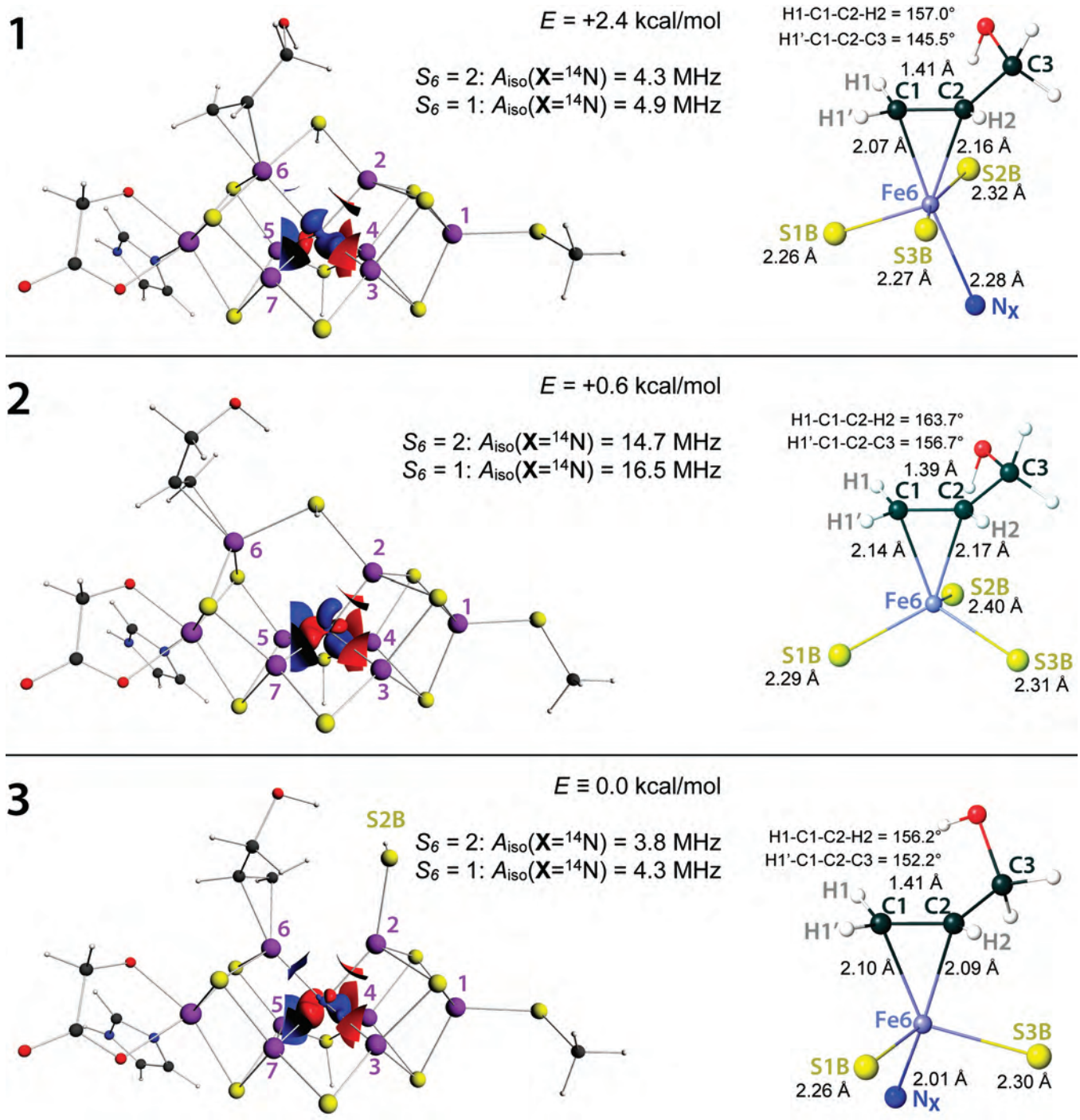

Figure 4. DFT-optimized model structures of allyl alcohol bound at Fe6 of FeMoco ($2e^-$ reduced state; μ^2S sulfurs S2B and S3A are protonated), illustrating electronic (**1**), structural (**2**), and complex (**3**) perturbation of the [6Fe] symmetry. The relative energies are reported. The calculated isotropic hyperfine couplings $A_{iso}(^{14}N_X)$ for the interstitial **X** = ^{14}N atom are given for the two options of the Fe6 site spin: $S_6 = 2$ (main assignment, canting at Fe6) and $S_6 = 1$ (alternative assignment, intermediate spin at Fe6, Figure 3). Point spin density isosurfaces inside the [6Fe] cage are shown using $\rho = \pm 0.005$ au isovalues. The coordination sphere of the Fe6 site is shown in detail, with Fe6−ligand distances reported. H1−C1−C2−H2 and H1′−C1−C2−C3 dihedral angles illustrate deviation of the bound ethylene fragment from the planar conformation.

bonding assignment. C1−C2 bond lengths of 1.41/1.39/1.41 Å obtained for **1/2/3**, see Figure 4, are closer to alkene C=C (1.34 Å) than to alkane C−C (1.54 Å) carbon−carbon bond length limit, which would again favor π-(C=C) bonding. There is, however, some degree of pyramidalization of the bound ethylene fragment, which can be characterized measuring H1−C1−C2−H2 and H1′−C1−C2−C3 dihedral angles (Figure 4), which are both equal to 179° in the optimized nonbound allyl alcohol, whereas H1−C1−C2−H2 = 157.0/163.7/156.2° and H1′−C1−C2−C3 = 145.5/156.7/152.2° were obtained for structures **1/2/3**. In summary, the geometric parameters of the Fe6-η^2(C=C) fragment are consistent with synergic bonding situation where the carbon atoms' hybridization is somewhat between sp^2 (corresponding to π-(C=C) bonding) and sp^3 (corresponding to σ-(C) bonding), with more preference to sp^2. The three ferracyclic

bonding distances we obtained for the Fe6-η^2(C═C) fragment (Figure 4) are very similar to those experimentally determined for the Pt-η^2(C═C) fragment in the classic olefin−metal complex, Zeise's salt ($K[PtCl_3(C_2H_4)]\cdot H_2O$): C1−C2 = 1.44 Å, Pt−C1 = 2.16 Å, Pt−C2 = 2.15 Å.[35]

The native FeMoco conformation is retained in the first considered structure **1** of Fe6-η^2(C═C) alkene coordination. The [6Fe] prismane structure in **1** is well retained, with only moderate elongation of Fe6−N_X by 0.3 Å with respect to the rest of Fe_i-N_X = 2.0 Å, i = 2...7, in [6Fe] (Table 2). The coordination of Fe6 in **1** can be considered as either pseudo trigonal bypyramidal (C═C fragment and N_X as axial, and S1B, S2B, S3B as equatorial ligands) or distorted octahedral (Figure 4). This Fe6 coordination is different from the rest of the tetrahedral iron sites in **1**. The difference in the coordination types causes inhomogeneity in spin populations: P(Fe6) = 1.1e versus the remaining irons which all bear $|P(Fe_i)| \geq 2.6e$ (Table 2). As previously proposed,[6] the dative π-(C═C) bonding here might yield intermediate- or low-spin iron. The calculated P(Fe6) = 1.1e likely corresponds to $M_{S_6} = 1$, which can be achieved via (i) canting of the high-spin $S_6 = 2$ ferrous site or (ii) its conversion into the true intermediate-spin $S_6 = 1$. **1** is therefore an intermediate, where largely the *electronic* (not structural) symmetry of the [6Fe] prismane is perturbed. The outcome of this perturbation is $A_{iso}(^{14}N_X) = 4.3$ MHz in the case of canting and $A_{iso}(^{14}N_X) = 4.9$ MHz in the case of the intermediate Fe6 spin (the spin projection factors used for $A_{iso}(\mathbf{X})$ are $P_X = 0.32$ ($S_6 = 2$) and 0.36 ($S_6 = 1$), correspondingly; section 3.2).

The FeMoco core is plastic and a Fe−N_X bond can be elongated significantly without a severe energetic penalty.[15,19] In the second optimized local minimum **2**, the coordination of N_X to Fe6 is lost: Fe6−N_X = 3.4 Å as compared to Fe−N_X ≤ 2.0 Å for the rest of the prismane irons. In contrast to **1**, Fe6 remains tetrahedral high-spin in **2**, exchanging the N_X ligand trans with the alkene, and $P(Fe_i)$ spin populations are relatively homogeneous. It is therefore primarily the *structural* [6Fe] symmetry perturbation that yields a large predicted $A_{iso}(^{14}N_X) = 14.7$ MHz calculated for **2** (using the spin projection factor $P_X = 0.32$).

In line with a proposal that a protonated μ_2S−H bridge opening at the substrate-binding iron site will facilitate the reduction,[19,36] Fe6−S2B coordination is no longer present in the third optimized conformation **3** of the allyl alcohol intermediate. There are no such prominent Fe−N_X or P(Fe) variations within [6Fe] obtained for **3** as those described above for **1** and **2**. $A_{iso}(^{14}N_X) = 3.8$ MHz calculated for **3** (using the spin projection factor $P_X = 0.32$) can therefore be considered as the result of combined *electronic and structural* [Fe6] symmetry perturbation.

The three modes of allyl alcohol binding to FeMoco considered above were found to be nearly equi-energetic. The order of the preference between the three local minima is as follows: **3** (≡0.0 kcal/mol), followed by **2** (+0.6 kcal/mol) and then by **1** (+2.4 kcal/mol). With such small energy differences for the present models, any of the above cofactor conformations may be found in the actual protein.

3.4. Iron Hyperfine Couplings. An alternative approach to discriminate between the three local minima **1**−**3** is to compare their semiempirical iron hyperfine parameters to the available ^{57}Fe ENDOR values of the (ethylene bound) S_{EPR1} state. We find S_{EPR1} relevant for the comparison because, like **1**−**3**, this FeMoco state presumably carries the Fe6-η^2(C═C) fragment. Using the derived K_i spin projection coefficients (section 3.2), semi-empirical iron isotropic hyperfine couplings A_i^{calcd} for allyl alcohol bound states **1**, **2**, and **3** are calculated via eq 6 and provided in Table 2. Four types of iron sites were reported for S_{EPR1} by ^{57}Fe ENDOR, with ±1 MHz uncertainty in A_i^{exptl} isotropic hyperfine couplings: (i) α_3, $A_i^{exptl} = 32$ MHz; (ii) α_4, $A_i^{exptl} = 33$ MHz; (iii) β_3, $A_i^{exptl} = 18$ MHz; (iv) β_4, $A_i^{exptl} = 23-26$ MHz.[6] The structural and electronic symmetry of the allyl alcohol-bound FeMoco suggests a distribution of the seven iron sites into four groups: (i) i = 1, unique terminal iron coordinating Cys275; (ii) i = 2, 3, 4, the only spin-down iron sites in BS2; (iii) i = 5, 7, spin-up iron sites in BS2 not binding the ligand; (iv) i = 6, the only ligand-binding iron site. Here, we infer that, because of the pseudo 3-fold rotational symmetry of BS2 FeMoco shown in Chart 2, iron numbers 2, 3, and 4 can be clustered into the group of three nearly equivalent sites; the ligand binding at Fe6 presumably results in splitting of the symmetry cluster arranged from iron numbers 5−7 into two groups, 5 & 7 and 6.

The occurrence of only four distinct iron hyperfine signals in S_{EPR1} is likely to impose selection rules on the possible allyl alcohol intermediate BS states. In section 3.1 above (and section 3.5 below), we find that BS2 and BS7 energies differ insignificantly and we need to provide additional arguments to discriminate between these states. Consistent with the ENDOR results, iron sites of BS2 can be separated into the four groups, as discussed in the previous paragraph. Using the similar approach for analyzing BS7, *five* groups of spectroscopic sites are expected, because the group of iron sites 2, 3, 4 equivalent in BS2 (all three spin-down) would now be split into two groups, 2 and 4 (spin-up) and 3 (spin-down) in BS7. For the ligand-bound FeMoco, this argument favors spin alignment BS2 versus BS7.

In Table 2, we provide the match between the above four groups of S_{EPR1} experimental A_i^{exptl} and our calculated A_i^{calcd} isotropic hyperfine couplings. Notably, the signs for A_i^{exptl} must be deduced from the spin coupling model because only the absolute values of hyperfine couplings can be obtained by ENDOR. In line with the previous approach,[6] we will restrict ourselves to assignments where only positive or only negative values are used for every observed type of A_i^{exptl}.

Whereas $a_{test} = -11$ to -14 MHz for the present assignment of S_{EPR1} ^{57}Fe ENDOR A_i^{exptl} data (measuring the quality of the iron hyperfine values, section 2.4) is slightly outside of the $-16 \leq a_{test} \leq -25$ MHz expected range, reasonably good overall fit was obtained. Notably, a_{test} values (obtained from the computed A_i^{calcd}, i = 2...7; Table 2) for the three local minima **1/2/3** are −19.7/−21.6/−20.6 MHz,

(35) Black, M.; Mais, R. H. B.; Owston, P. G. *Acta Crystallogr., Sect. B* **1969**, *25*, 1753.
(36) Kastner, J.; Blochl, P. E. *Inorg. Chem.* **2005**, *44*, 4568–75.

respectively, which is in the middle of the expected a_{test} range. The major difference between A_i^{calcd} value sets for structures **1**−**3** is observed at the Fe6 ligand-binding site: −9.9 MHz for **1**, −26.9 MHz for **2**, and −18.2 MHz for **3**. $|A_i^{exptl}| = 18$ MHz assigned to Fe6 β_3 site apparently favors structure **3** of the allyl alcohol intermediate. An alternative assignment of $|A_i^{exptl}|$ values, exchanging β_3 and β_4 sites between Fe1 and Fe6 (Table 2), would favor structure **2** with $A_i^{exptl} = -23$ to −26 MHz (β_4) for Fe6. However, this would produce much worse correspondence between A_i^{calcd} and $|A_i^{exptl}|$ at the terminal Fe1 site, for which our calculated values are in the −25.4 to −27.1 MHz range, and the experimental value of the alternative assignment would be −18 MHz (β_3). Structure **1** has a very low $A_6^{calcd} = -9.9$ MHz value resulting from the corresponding low covalency factor at Fe6, $d_B(Fe_6) = 0.27$. In summary, iron hyperfine properties analysis for the coupling where Fe6 ferrous spin is canted ($S_6 = 2$, $M_{S_6} = 1$) is most consistent with the following order of preference between the three local minima: **3**, followed by **2**, and then by **1**.

Consideration of an alternative spin coupling model where Fe6 converts to the intermediate spin ($S_6 = 1$ vs canted $S_6 = 2$, sections 3.2 and 3.3) would actually favor structure **1** of the Fe6-η^2(C═C) intermediate. Only this local minimum passes the covalency factor test ($d_B(Fe_i) < 1$, section 2.4) for Fe6. Only for **1** does an intermediate spin at Fe6 yield a reasonable hyperfine $A_6^{calcd} = -14.8$ MHz (Table S2 in the Supporting Information). For **2** and **3**, the calculated covalency factors are $d_B(Fe_6) = 1.48$ and 1.00, correspondingly (Table S3 in the Supporting Information). Via eq 6, large $d_B(Fe_6)$ also results in $A_6^{calcd} = -40.4$ and −27.3 for **2** and **3**, correspondingly, which significantly deviate from the assigned $A_i^{exptl} = -18$ MHz (Table S2 in the Supporting Information). Moreover, $a_{test} < -30$ MHz for all the three local minima when using the alternative coupling are too negative, when compared to $a_{test} = -11$ to −14 MHz of the fitted ^{57}Fe ENDOR values and also to the $-16 \le a_{test} \le -25$ MHz expected range.

One more alternative assignment for the iron site hyperfine parameters accompanies the ^{57}Fe ENDOR study of S_{EPR1} state.[6] This assignment, largely based on the best fit of −17 to −20 MHz to a_{test}, is as follows: (i) α_3, $A_i^{exptl} = -32$ MHz, 1 × $Fe^{2.5+}$; (ii) α_4, $A_i^{exptl} = -33$ MHz, 1 × $Fe^{2.5+}$; (iii) β_3, $A_i^{exptl} = 18$ MHz, 4 × Fe^{2+}; (iv) β_4, $A_i^{exptl} = -23$ to −26 MHz, 1 × Fe^{2+}. All iron sites were proposed to be high-spin. According to eqs 3 and 6, spin-up sites correspond to negative A_i^{calcd} and spin-down sites correspond to positive A_i^{calcd}. The earlier assignment would therefore exhibit a 3↑:4↓ spin coupling of the seven FeMoco iron sites, called the BS− state here. However, our present results favor 4↑:3↓ spin coupling (namely, BS2); as explained above, a 3↑:4↓ spin coupling is accessible for the $2e^-$ reduced $S = 1/2$ cofactor only when at least *two* $M_{S_i} = 1$ (intermediate spin) or highly canted Fe^{2+} sites are present.

3.5. Alternative Spin Couplings for the Ligand-Bound States. Allyl alcohol binding in structures **1**−**3** provides a substantial electronic and structural perturbation to the [Mo−7Fe−9S−**X**] core, as reflected in Table 2 and Figure 4. Tentative usage of BS2 spin coupling for states **1**−**3** in section 3.3 above thus needs additional justification: whereas we show that BS2 is the lowest-energy state for the free $2e^-$ reduced FeMoco (section 3.1 and Chart 2), alternative spin couplings might be preferred when a ligand binds at Fe6. To avoid an excessive number of calculations, we provide a limited exploration of the BS space for structures **1**−**3**: only the three most stable spin couplings, as obtained from the free $2e^-$ reduced FeMoco analysis, will be considered. These couplings are BS2 (≡0.0 kcal/mol), BS7 (0.2 kcal/mol), and BS6 (3.3 kcal/mol). The relative energies for the resulting optimized 9 states (3 structures × 3 spin couplings = 9 states) are compared in parts a−c in Table S5 in the Supporting Information. From part b in Table S5 in the Supporting Information, it can be deduced that, for all the three spin couplings considered, local minimum **3** remains more stable than **1** or **2**. Part c of Table S5 in the Supporting Information shows that BS2 is the most-stable spin coupling for local minima **1** and **2**; for **3**, BS7 is the most stable coupling, with BS2 only 1.6 kcal/mol above BS7. In summary, for allyl alcohol bound FeMoco species, the above results support (i) structure **3** as the most stable local minima and (ii) BS2 and BS7 as the generally most-preferred spin couplings based on the relative energies.

Calculated central atom hyperfine parameter $A_{iso}(^{14}N_X)$ for the above nine states (Table S6 in the Supporting Information) all show significant increase as compared to the resting state $A_{iso}(^{14}N_X) = 0.3$ MHz value obtained earlier.[8] For the three alignments BS2, BS6, and BS7, the observed trend in magnitude of $A_{iso}(^{14}N_X)$ is an increase in the **3** < **1** < **2** order. For simplicity, when calculating the **X** hyperfine value for BS6 and BS7 alignments, we used the same spin projection factor $P_X = 0.32$ as derived below in section 3.2 for BS2.

4. Conclusions

BS-DFT calculations have been used to address the $2e^-$ reduced state of the FeMoco cofactor of nitrogenase. The calculations provide a framework for understanding the [Mo−7Fe−9S−**X**] core electronic structure in freeze-trapped $S = 1/2$ paramagnetic states observed when various ligands coordinate to FeMoco.

We have used a new combinatorial approach that generates all of the possible spin configurations of the metal sites (BS states) compatible with their given bulk oxidation level and total spin. For $2e^-$ reduced $S = 1/2$ FeMoco, we show that ten 4↑:3↓, ten 3↑:4↓, and six 5↑:2↓ spin couplings of the seven iron sites are available (Chart 2). Combined consideration of the relative energies, FeMoco symmetry, and comparison of the calculated versus experimental iron hyperfine parameters favor BS2 (one of the 4↑:3↓ couplings) as the most appropriate spin alignment from the BS pool.

The three local minima **1**−**3** (Figure 4) considered for the allyl alcohol intermediate all share Fe6-η^2(C═C) ferracycle mode of the ligand binding (Chart 1), where Fe6−C π-(C═C) bonding character was found to prevail over σ-(C). **1**, **2**, and **3** illustrate the following three types of [6Fe] FeMoco iron prismane perturbation (Table 2): (i) minor structural effects but significant electronic influence on the

Fe6 spin state in **1**; (ii) dissociation of the Fe6−**X** bond in favor of the Fe6−ligand bond trans to it, with little change of the Fe6 spin state in **2**; (iii) opening of the protonated μ_2S2B−H bridge from the Fe6 side, introducing a moderate level of both structural and electronic perturbation in **3**. Calculated relative energies and iron hyperfine parameters suggest that **3** is the most favored binding mode, followed by **2**, and then by **1**.

The comparison of the BS-DFT semiempirical versus ^{57}Fe ENDOR experimental iron hyperfine coupling parameters for the Fe6-η^2(C═C) intermediate support the spin coupling, where the ligand-binding Fe6 site is canted high-spin ($S_6 = 2$, $M_{S_6} = 1$) ferrous ion (Tables 1 and 2); $A_6^{\text{calcd}} = -18.2$ MHz (for the allyl alcohol binding mode **3**) is then in the good agreement with the smallest $A_i^{\text{exptl}} = 18$ MHz reported for S_{EPR1} (which is FeMoco freeze-trapped spectroscopic state with C_2H_4 bound). An alternative spin coupling model assigning true intermediate spin to Fe6 ($S_6 = 1$, $M_{S_6} = 1$) would pass the Fe6 covalency factor test ($d_B(Fe_i) < 1$, section 2.4) only for structure **1** among the three alternatives analyzed. Whereas the corresponding $A_6^{\text{calcd}} = -14.8$ MHz is reasonable, the $S_6 = 1$ assignment results in too negative $a_{\text{test}} < -30$ MHz (Table S2 in the Supporting Information) values for all of the three allyl alcohol binding modes.

One further extension of our study is the analysis of the hyperfine parameters for allyl alcohol atoms when bound to the $S = {}^1/_2$ cofactor. The experimental ^{13}C and ^{1,2}H ENDOR characterization for this FeMoco ligand is already available.[14] Our preliminary results are that the ligand hyperfine parameters are significantly sensitive to (i) the ligand orientation relatively to FeMoco and (ii) hydrogen bonding to the ligand atoms from the protein environment. The reported pH dependence of the allyl alcohol intermediate EPR signal intensity was interpreted in favor of the hydrogen bonding between the protonated His195 imidazole and allyl-OH oxygen.[12,13] BS-DFT calculations incorporating His195 into the model are in progress.

A major conclusion of the present study is that coordination of a ligand at one of the [6Fe] prismane irons most likely perturbs the symmetry in such a way that $A_{\text{iso}}(\mathbf{X})$ increases at least 1 order of magnitude ($A_{\text{iso}}(^{14}N_{\mathbf{X}}) = 4.3/14.7/3.8$ MHz for structures **1/2/3**, correspondingly), as compared to the ligand-free resting state FeMoco ($A_{\text{iso}}(^{14}N_{\mathbf{X}}) = 0.3$ MHz; section 1). Shown for **X** = N, this trend is likely to be qualitatively correct for other **X** alternatives carbon and oxygen. In summary, certain ligands coordinating to FeMoco are expected to generate **X** hyperfine signal large enough to be detected, and differentiated from the protein atoms, by techniques such as ENDOR and ESEEM. An experimental examination of this computational result, capable of casting light on the identity of **X**, is anticipated.

Acknowledgment. We acknowledge the financial support by NIH Grant GM39914 (to DAC and L.N.). We thank E. J. Baerends for ADF codes, W.-G. Han for computational assistance, and B. M. Hoffman for valuable discussions.

Supporting Information Available: Details of the alternative spin coupling, covalency factors for the iron sites, net electron spin populations for the noniron FeMoco core atoms, relative energies and $A_{\text{iso}}(\mathbf{X} = {}^{14}N)$ values for the allyl alcohol bound FeMoco structures **1**−**3** in BS2, BS6, and BS7 spin alignments, and optimized XYZ coordinates for **1**−**3**. This material is available free of charge via the Internet at http://pubs.acs.org.

IC7022743